



OPEN ACCESS

EDITED BY
Jeffrey Dome,
Children's National Hospital, United States

REVIEWED BY
Rodrigo LP Romao,
Dalhousie University, Canada
Han Lv,
Department of Radiology, Capital Medical
University, China

*CORRESPONDENCE
Tianye Niu
✉ tyniu@qq.com
Qiang Shu
✉ shuqiang@zju.edu.cn

†These authors have contributed
equally to this work and share
first authorship

SPECIALTY SECTION
This article was submitted to
Pediatric Oncology,
a section of the journal
Frontiers in Oncology

RECEIVED 12 December 2022
ACCEPTED 10 April 2023
PUBLISHED 20 April 2023

CITATION
Ma X-H, Yang J, Jia X, Zhou H-C,
Liang J-W, Ding Y-S, Shu Q and Niu T
(2023) Preoperative radiomic signature
based on CT images for noninvasive
evaluation of localized nephroblastoma in
pediatric patients.
Front. Oncol. 13:1122210.
doi: 10.3389/fonc.2023.1122210

COPYRIGHT
© 2023 Ma, Yang, Jia, Zhou, Liang, Ding, Shu
and Niu. This is an open-access article
distributed under the terms of the [Creative
Commons Attribution License \(CC BY\)](#). The
use, distribution or reproduction in other
forums is permitted, provided the original
author(s) and the copyright owner(s) are
credited and that the original publication in
this journal is cited, in accordance with
accepted academic practice. No use,
distribution or reproduction is permitted
which does not comply with these terms.

Preoperative radiomic signature based on CT images for noninvasive evaluation of localized nephroblastoma in pediatric patients

Xiao-Hui Ma^{1†}, Jing Yang^{2,3†}, Xuan Jia¹, Hai-Chun Zhou¹,
Jia-Wei Liang¹, Yu-Shuang Ding¹, Qiang Shu^{1*}
and Tianye Niu^{4,5*}

¹The Children's Hospital, Zhejiang University School of Medicine, National Clinical Research Center for Child Health, Hangzhou, Zhejiang, China, ²Women's Hospital, Zhejiang University School of Medicine, Hangzhou, Zhejiang, China, ³Institute of Translational Medicine, Zhejiang University, Hangzhou, Zhejiang, China, ⁴Institute of Biomedical Engineering, Shenzhen Bay Laboratory, Shenzhen, China, ⁵Peking University Aerospace School of Clinical Medicine, Aerospace Center Hospital, Beijing, China

Background: Nephron sparing nephrectomy may not reduce the prognosis of nephroblastoma in the absence of involvement of the renal capsule, sinus vessels, and lymph nodes. However, there is no accurate preoperative noninvasive evaluation method at present.

Materials and methods: 105 nephroblastoma patients underwent contrast-enhanced CT scan between 2013 and 2020 in our hospital were retrospectively collected, including 59 cases with localized stage and 46 cases with non-localized stage, and then were divided into training cohort (n= 73) and validation cohort (n= 32) according to the order of CT scanning time. After lesion segmentation and data preprocessing, radiomic features were extracted from each volume of interest. The multi-step procedure including Pearson correlation analysis and sequential forward floating selection was performed to produce radiomic signature. Prediction model was constructed using the radiomic signature and Logistic Regression classifier for predicting the localized nephroblastoma in the training cohort. Finally, the model performance was validated in the validation cohort.

Results: A total of 1652 radiomic features have been extracted, from which TOP 10 features were selected as the radiomic signature. The area under the receiver operating characteristic curve, accuracy, sensitivity and specificity of the prediction model were 0.796, 0.795, 0.732 and 0.875 for the training cohort respectively, and 0.710, 0.719, 0.611 and 0.857 for the validation cohort respectively. The result comparison with prediction models composed of

different machine learning classifiers and different parameters also manifest the effectiveness of our radiomic model.

Conclusion: A logistic regression model based on radiomic features extracted from preoperative CT images had good ability to noninvasively predict nephroblastoma without renal capsule, sinus vessel, and lymph node involvement.

KEYWORDS

nephroblastoma, radiomics, machine learning, predictive modeling, localized stage

Introduction

Nephroblastoma, also known as Wilms tumor, is the most common renal tumor in pediatric patients (1), accounting for more than 90% of all malignant kidney tumors in children (2), it is also the most frequent pediatric abdominal malignant tumor and the fourth most frequent pediatric malignant tumor overall (3). Under the comprehensive treatment of surgery, chemotherapy, and radiotherapy, the five-year survival rate of nephroblastoma patients has exceeded 90% (4). The current focus of treatment is on how to better protect kidney function and improve long-term survival quality based on ensuring survival rates.

Nephron sparing surgery (NSS) helps to protect the kidneys in the long term and prevent the development of chronic kidney disease, which is especially important in children with a long survival period and facing progressive renal insufficiency (5, 6). Since the successful application in bilateral nephroblastoma, NSS has also been increasingly used to remove selected cases of unilateral nephroblastoma (7–9). Studies have found that in the group of patients with localized disease, the event-free survival and overall survival after NSS appeared to be as good as after total nephrectomy (TN), and local recurrence rates were the same as after TN (8). The application of NSS in unilateral nephroblastoma is limited due to the possible risk of recurrence caused by positive margins. If nephroblastoma patients without the involvement of renal capsule, sinus vessels, and lymph nodes (named localized stage here) can be accurately distinguished before surgery, it will be of great significance to the management of nephroblastoma and will promote the precision treatment of nephroblastoma.

Radiomics is a novel technology that can extract a large number of quantitative information describing the pathophysiological status and phenotypic characteristics of lesions from CT, PET, MRI and other medical images (10–12). Models can be built through in-depth analysis of the extracted mineable radiomic features, combined with clinical examinations and testing information, and using suitable machine learning algorithms to provide clinical decision support. It has shown great advantages in metastasis prediction (13), tumor diagnosis (14), treatment response evaluation (15), and prognosis analysis (16).

The purpose of this study is to establish a radiomic approach based on CT images to develop a non-invasive tool for preoperative prediction of localized nephroblastoma of pediatric patients.

Materials and methods

Patients and study flow diagram

This retrospective study was approved and the requirement for informed consent was waived by the Institutional Review Board of our participating institution (Children's Hospital of Zhejiang University School of Medicine, Zhejiang, China). Inclusion criteria are: (a) computed tomography (CT)-enhanced abdominal scan before surgery, biopsy, radiotherapy, or chemotherapy; (b) successful tumor resection; (c) postoperative pathology proved to be nephroblastoma. Exclusion criteria are: (a) Contrast-enhanced CT imaging of the tumor was not accomplished or treatment was performed before CT scanning; (b) CT images were poor (e.g. motion artifacts); (c) Radiotherapy, chemotherapy or both were applied prior to surgery; (d) Pathology was unclear; (e) bilateral nephroblastoma. We retrospectively collected 105 patients diagnosed as nephroblastoma from December 2013 to September 2020. There are 59 patients in non-localized stage and 46 patients in localized stage. These patients were divided into the training and validation cohorts according to the order of CT scanning time (training cohort, December 2013 to March 2019; validation cohort, April 2019 to September 2020). The training cohort and the validation cohort consist of 73 patients and 32 patients, respectively. Details of our dataset in this study are provided in Table 1. The flow diagram of this radiomics study consists of lesion

TABLE 1 Details of our dataset in this study.

	Training cohort	Validation cohort	Total
localized	41	18	59
Non-localized	32	14	46
Total	73	32	105

segmentation, data preprocessing, feature extraction, feature selection and model construction. More details are provided below.

Definition of localized and non-localized stage

Localized stage refers to stage I of the COG nephroblastoma staging system1, excluding items related to surgery.

- Tumor is limited to the kidney.
- The renal capsule is intact.
- The tumor is not ruptured or biopsied before being removed.
- No involvement of renal sinus vessels.
- All lymph nodes sampled are negative.

All the other cases were considered as non-localized stage, equivalent to preoperative stage II-V.

Both localized and non-localized stage were identified based on postoperative pathology.

CT image acquisition and lesion segmentation

Before CT examination, all of the patients were asked to fast for 4 to 6 hours. Somatom Emotion 16 (SIEMENS) and Optima CT660 CT (GE Medical Systems) were used for examination. Scanning parameters of Somatom Emotion 16 CT scanner were tube voltage 110 kV, tube current 75 mA, layer thickness 1.5 mm, field of view (FOV) 350mm × 350 mm, matrix 512 × 512. Parameters of GE

Optima CT660 CT were tube voltage 120 kV, tube current 80 mA, layer thickness 0.625 mm, FOV 350mm × 350 mm, and matrix 512 × 512. High pressure syringe (Mallinckrodt Injection System, Liebel-Flarsheim Co.) was used for nonionic iodine contrast agent injection according to body weight (1.5 ml/kg) at a rate of 1.5-2 ml/s. Portal venous phase images were scanned 50s after the injection.

Portal venous phase CT images were uploaded to a secure laptop. Then 3-Dimensional Slicer (3DSlicer, 4.11.0, <http://www.slicer.org/>) was used to delineate the three-dimensional (3D) regions of the renal masses with a semi-automatic segmentation procedure, which was performed by two senior radiologists who had more than 10 years of clinical experience. Both of the results they obtained were used to extract radiomic features for evaluating inter- and intra- observer repeatability through Intra Class Correlation Coefficient (ICC).

Data preprocessing and feature extraction

Volume of interest (VOI) including the whole mass of each nephroblastoma patient was segmented according to radiologists' delineation (Figure 1), then, VOI of all the images were resampled and gray-level normalized by PyRadiomics before feature extracting. We utilized the nearest neighbor algorithm to interpolate each VOI into isotropic data. The voxel spacing of our isotropic data was set to 1×1×1 mm³, 3×3×3 mm³, or 5×5×5 mm³.

Radiomic features were extracted from original and derived interpolated VOIs using PyRadiomics v2.2.0 (17), an open-source python package (<https://pyradiomics.readthedocs.io/en/latest/>). These derived interpolated VOIs were obtained by applying six built-in optional filters (including Laplacian of Gaussian, Wavelet, Square, Square Root, Logarithm and Exponential) to original

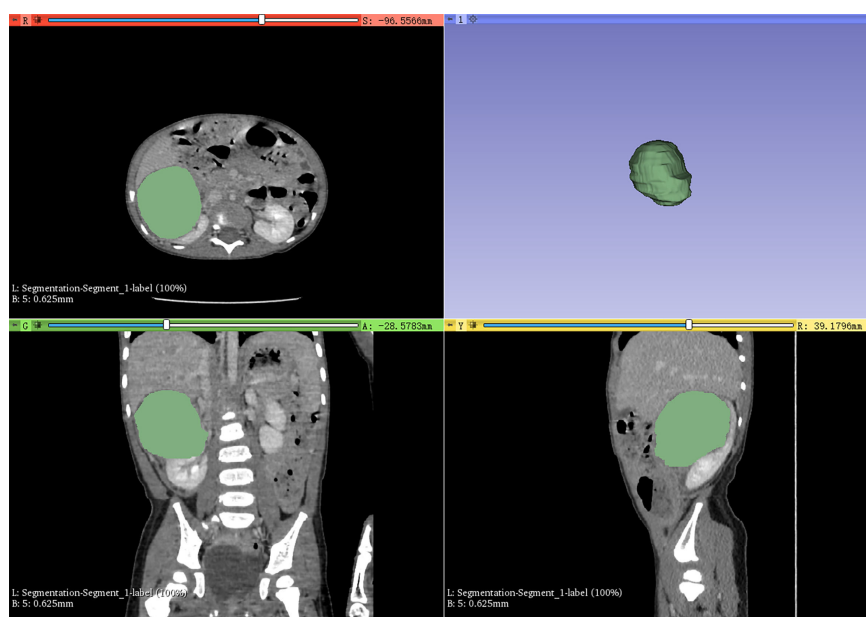


FIGURE 1

3D-Slicer was used to semi-automatically delineate the whole mass as the volume of interest for radiomics feature extraction.

interpolated VOIs. Feature classes consist of shape, first order statistics and texture features. Texture features contain gray level cooccurrence matrix (GLCM), gray level run length matrix (GLRLM), gray level size zone matrix (GLSZM), neighbouring gray tone difference matrix (NGTDM), and gray level dependence matrix (GLDM) features. All radiomic features were normalized (Z-score) to balance the feature contribution and make each feature at the same quantity level. All feature classes with the exception of shape can be extracted on original and derived interpolated VOIs.

Feature selection and model construction

In this study, we devised a multi-step procedure for the selection of radiomic features to produce radiomic signature. First, Pearson correlation analysis (13, 18, 19) was used to identify the redundancy of radiomic features in the training cohort. We calculated Pearson correlation coefficients of pair-wise radiomic features to build Pearson correlation matrix. Each feature with the mean absolute correlation higher than Pearson threshold was considered redundant thus eliminated. The Pearson threshold between 0.70 and 0.95 (the stride was 0.5) was utilized to identify the highly correlated feature pairs. Then the radiomic signature was identified by sequential forward floating selection (SFFS) algorithm (20). We utilized Logistic Regression (LR), ten-fold cross validation, and area under the receiver operating characteristic (ROC) curve (AUC) value as the classifier, K-fold cross validation, scoring criterion of the SFFS algorithm respectively. The number of retained features varies from 1/15 to 1/10 of total patient sample size (the stride was 1) (21–23), that is, the number of retained radiomic features ranged from 7 to 11. Next, the corresponding radiomic signature of the validation cohort were obtained according to the radiomic signature of the training cohort.

Considering the voxel spacing of isotropic data, the Pearson threshold and the number of retained features vary the radiomic signature, we constructed prediction models with different

parameters and LR classifier to classify patients with localized and non-localized nephroblastoma in the training cohort. The discrimination performance was quantified by the AUC value. In addition to the LR classifier, we further compared the performances of prediction models using the optimal parameter combination and other machine learning classifiers. These classifiers include Support Vector Machine with Recursive Feature Elimination (SVM-RFE), Random Forest (RF), Adaptive Boosting (AdaBoost), Gradient Boosting Decision Tree (GBDT), and eXtreme Gradient Boosting (XGBoost). Finally, the performance was validated in the validation cohort. The flow chart was shown in Figure 2.

Results

A total of 105 patients (50 males/55 females) were enrolled in the study, including 59 cases with non-localized stage and 46 cases with localized stage. They were divided into training cohort (n= 73, 37 males/36 females) and validation cohort (n= 32, 13 males/19 females) according to the order of CT scanning time. Age of the total study sample ranged from 0.1 to 10.3 years, with a median age of 2.1 years. Age of the training cohort ranged from 0.1 to 7.9 years with a median age of 1.9 years, whereas age of the validation cohort ranged from 0.1 to 10.3 years with a median age of 2.9 years.

A total of 1652 radiomic features have been extracted on each VOI. For original interpolated VOIs, 105 radiomic features were obtained including 14 shape features, 18 first order statistics features and 73 texture features. The remaining 1547 radiomic features were extracted from derived interpolated VOIs. They consisted of 306 first order statistics features and 1241 texture features. ICC analysis showed that the radiomic features from the VOIs delineated by the two senior radiologists had good inter- and intra- observer repeatability (ICC ranged from 0.73 to 1.0).

In order to determine the optimal parameter combination, we have adjusted different parameters (including the voxel spacing of isotropic data, the Pearson threshold and the number of retained

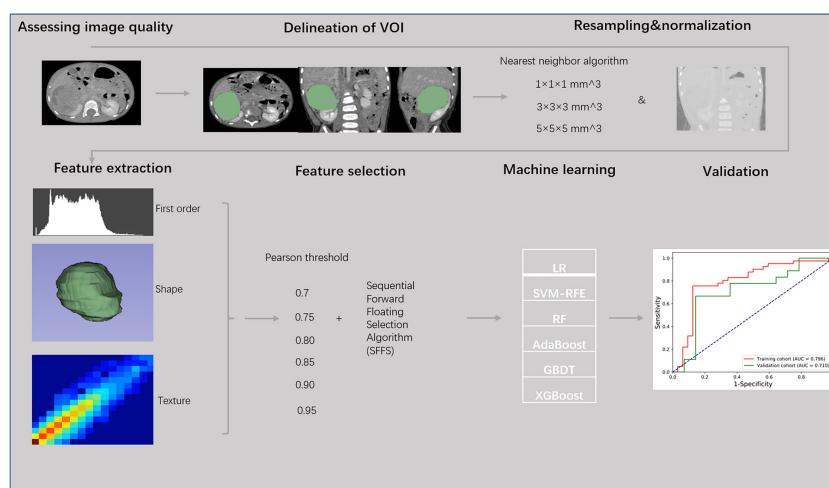


FIGURE 2 Flow chart of radiomics analysis of localized nephroblastoma.

features) and then established the corresponding LR models in the training cohort. The LR model with the optimal parameter combination was chosen as the final LR model. We found that the optimal parameter combination was the voxel spacing of 1×1×1 mm³, the Pearson threshold of 0.90 and the feature number of 10. When one parameter remains unchanged and other parameters change, the AUC values of the LR models are shown in Figure 3. The AUC value decreases with the increase of the voxel spacing of isotropic data, illustrating that clearer image data is more conducive to radiomics analysis. A total of 11 patients (including 4 cases of non-localized stage and 7 cases of localized stage) were able to correctly predict whether they were localized or not, even if the voxel spacing was changed. As for the Pearson threshold and the number of retained features, no clear pattern was observed in this single-center study. In the Pearson correlation analysis, a total of 354 radiomic features (including 3 shape features, 73 first order statistics features and 278 texture features) were obtained with threshold 0.90. About 78.57% of radiomic features have been eliminated. After the SFFS feature-ranking algorithm, top 10 radiomic features (including 3 first order statistics features and 7 texture features) were selected as our radiomic signature (Table 2).

In addition to the final LR model, SVM-RFE, RF, AdaBoost, GBDT, and XGBoost models were constructed using the optimal parameter combination and the corresponding machine learning classifiers. Table 3 shows the AUC values of these models for predicting the localized status in patients with nephroblastoma. Although the same radiomic signature was used, only AUC values of the final LR model were higher than 0.70 in the training and validation cohorts (training cohort, 0.796; validation cohort, 0.710). Other prediction models performed poorly in distinguishing localized group from non-localized group. It designates the potential of LR-based radiomics in classifying localized and non-localized nephroblastoma in pediatric patients. For the final LR model, the radiomic signature calculation formula is presented as follows: Rad_ signature = 0.22 - 0.52 × Feature_1 - 0.56 × Feature_2 - 0.21 × Feature_3 - 0.35 × Feature_4 - 0.84 × Feature_5 - 0.02 × Feature_6 + 0.58 × Feature_7 + 0.27 × Feature_8 + 0.33 × Feature_9 - 0.31 × Feature_10.

We further explored the performances of our radiomic signature calculation formula based on the final LR model using

TABLE 2 Details of the radiomic signature in this study.

Feature	Image Type	Feature Class	Specific Name
Feature_1	Log-sigma-5-0-mm-3D	NGTDM	Strength
Feature_2	Wavelet-HLH	GLSZM	LargeAreaLowGrayLevelEmphasis
Feature_3	Wavelet-HHH	GLCM	ClusterShade
Feature_4	Wavelet-HHH	GLSZM	GrayLevelNonUniformity
Feature_5	Wavelet-LLL	Firstorder	Maximum
Feature_6	Square	Firstorder	Kurtosis
Feature_7	Square	GLSZM	SmallAreaEmphasis
Feature_8	Square	GLSZM	ZoneVariance
Feature_9	Logarithm	GLCM	ClusterProminence
Feature_10	Exponential	Firstorder	Kurtosis

“Log-sigma-5-0-mm-3D” means that the 3D Laplacian of Gaussian filter with the kernel width “sigma” of 5.0 was implemented. “Wavelet-HLH” means that a high-pass filter, a low-pass filter and a high-pass filter was applied on x, y and z-axis of the wavelet filter, which was named analogously for “Wavelet-HHH” and “Wavelet-LLL”. “Firstorder” means first order statistics.

more performance metrics (such as accuracy, sensitivity and specificity). All performance metrics of the final LR model for predicting the localized nephroblastoma are presented in Figure 4. The AUC, accuracy, sensitivity and specificity are 0.796, 0.795, 0.732 and 0.875 for the training cohort respectively, and 0.710, 0.719, 0.611 and 0.857 for the validation cohort respectively. Results manifest the effectiveness in distinguishing patients with localized and non-localized nephroblastoma (Figure 5).

Discussion

The overall survival outcomes of most nephroblastoma patients are good, and further studies should focus on how to use the

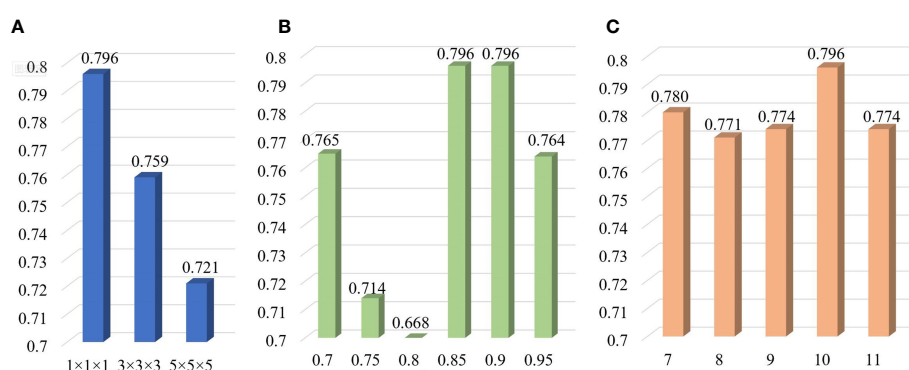


FIGURE 3 AUC values of LR models with various parameters including the voxel spacing of isotropic data (A), the Pearson threshold (B) and the number of retained features (C) in the training cohort.

TABLE 3 AUC values of different prediction models for predicting the localized nephroblastoma.

Model	Training cohort	Validation cohort
LR	0.796	0.710
SVM-RFE	0.697	0.808
RF	0.643	0.657
AdaBoost	0.531	0.619
GBDT	0.608	0.647
XGBoost	0.643	0.694

optimal treatment under more precise risk-stratified strategies (24) to improve the long-term prognosis of patients with nephroblastoma. Our result can be regarded as a kind of non-invasive risk-stratified strategies prior to surgery for nephroblastoma patients using radiomics technique, which goes beyond the ability of the human eye to identify the completely localized status in CT images.

Unlike previous surveys that concerned of all stages of nephroblastoma, our current study highlighted on the detection of nephroblastoma patients at a very early stage without involvement of renal capsule, sinus vessels, and lymph nodes. These patients can not only undergo complete tumor resection, but also have the potential to perform nephron sparing nephrectomy. Therefore, we developed a new method to divide patients into localized group and non-localized group non-invasively before operation, so as to guide the personalized treatment of nephroblastoma. To the best of our knowledge, the relationship between radiomic features and the involvement of renal capsule, sinus vessels, and lymph nodes of nephroblastoma has not been evaluated previously.

At present, lots of studies have shown that radiomic technology has the power to predict metastasis of different diseases. For example, one of our previous studies showed that radiomic features could effectively predict preoperative lymph node metastasis in patients with gastric cancer (13). In that study,

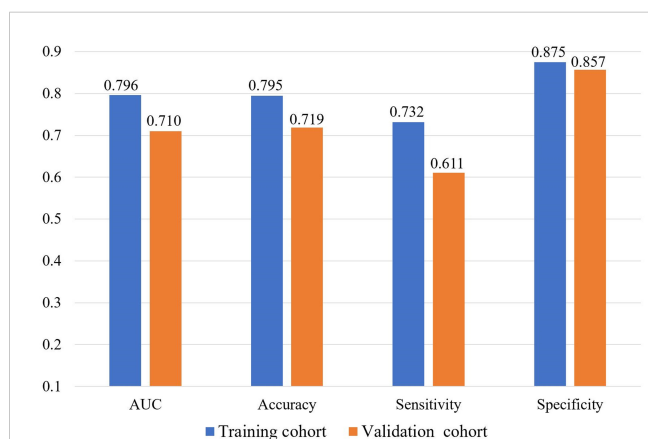


FIGURE 4 Performances of the final LR model for predicting the localized nephroblastoma.

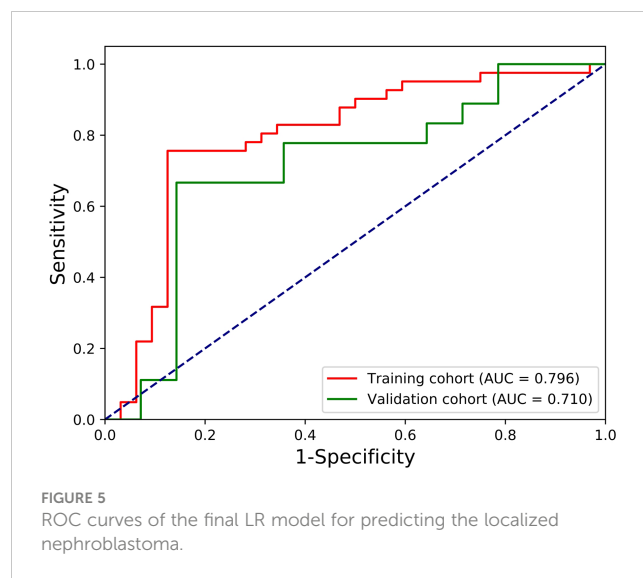


FIGURE 5 ROC curves of the final LR model for predicting the localized nephroblastoma.

tumor radiomics and LN radiomics were integrated to build an effective non-invasive tool to guide treatment decision-making in gastric cancer, which was notably useful in patients with T2-stage, diffuse subtype, and moderately/well differentiated gastric cancer. Zhao et al. found that radiomic features from preoperative CT images could predict future distant metastasis of local renal cell carcinoma after surgical resection, and these predictive radiomic features were related to certain important biological pathways (extracellular matrix-receptor interaction, focal adhesion and Phosphoinositide 3-kinases/Akt pathways) (25). Their study suggested that these findings provided support for the biological interpretation of radiomics model and might enhance the molecular basis of radiomics. Both of the above studies showed that the radiomic technology has offered a possible solution for studying the correlation between medical imaging and tumor metastasis in patients with nephroblastoma.

In this study, we found that the radiomic features extracted from enhanced CT images of preoperative nephroblastoma patients could be used as an independent predictor of localized nephroblastoma. 10 radiomic features related to early localized stage of nephroblastoma were screened out from a large amount of data through a generalized methodology for radiomic feature selection and modeling developed by our team (23), in which Pearson correlation analysis and SFFS algorithm were used for feature selection. The methodology was verified by our own three data sets (Gastric cancer dataset, Osteosarcoma dataset, Pancreatic neuroendocrine tumors dataset) and performed well in these three different origin and different types of solid tumors, which proves the stability and reliability of this methodology in feature selection. Similarly, the results of our LR-based model in this study demonstrated the effectiveness of radiomic features based on preoperative enhanced CT images for predicting localized nephroblastoma at the training cohort (AUC, 0.796; accuracy, 0.795; sensitivity, 0.732; specificity, 0.875) and the validation cohort (AUC, 0.710; accuracy, 0.719; sensitivity, 0.611; specificity, 0.857).

In addition to a single machine learning classifier, the performance of different classifiers based on same radiomic features was also worth exploring. Parmar et al. found that classifiers had a significant impact on the model performance (accounting for 34.21% of the total model differences) (26), so it was a very important step to determine the best machine learning classifier and apply it to radiomics. Our results also supported this conclusion. Through the comparison of 6 machine learning classifiers (LR, SVM-RFE, RF, AdaBoost, GBDT, and XGBoost), we found that LR was the most suitable classifier for our dataset –only the AUC of LR was higher than 0.75 in training cohort (training cohort: 0.796), and it performed equally well on the validation cohort (validation cohort: 0.710). Dong et al. applied multiple machine learning methods based on radiomics to differentiate intracranial ependymoma from medulloblastoma and found that the performance of RF classifier was the best (AUC 0.91, 95% CI 0.787–0.968), followed by Support Vector Machines and K neighbors, and Adaboost was the worst (AUC 0.75, 95% CI 0.604–0.857) (27). Then Paired test showed significant difference ($P < 0.05$) in ROC curve among the classifiers used. In this study, we also compared the model performance of LR with other machine learning methods, which used the same radiomic features for predicting the absence of involvement of the renal capsule, sinus vessels, and lymph nodes in nephroblastoma. The results illustrated that the radiomic model of LR achieved the best performance both in the training cohort and validation cohort ($P < 0.05$).

By comparing radiomic features based on three different types of interpolated images, it was found that features extracted from images with the smallest voxel spacing ($1 \times 1 \times 1 \text{ mm}^3$) resulted in the best model accuracy, which was consistent with the truth that smaller voxel associated with the higher resolution (28), even though this smaller voxel was obtained by a resampling technique.

Despite the aforementioned important findings, our study still had several limitations. First of all, this study was retrospective and had a relatively small size of cohort, although external validation was used. In order to obtain a higher level of clinical application evidence, it needed to be verified with prospective and larger data sets. Secondly, our study did not take into account some other features, such as clinical features, genomics and so on. The combination of multi-dimensional data may further improve the predictive ability of the model and thus providing better clinical decision support.

Overall, the results showed that the LR-based radiomic model had a good ability of non-invasive prediction of nephroblastoma without renal capsule, sinus vessels and lymph node involvement, and had the potential to help make surgical decisions for precise treatment and improve the long-term quality of life of nephroblastoma patients. However, more data is needed to improve the global applicability and robustness of the method.

Data availability statement

The original contributions presented in the study are included in the article/supplementary material. Further inquiries can be directed to the corresponding authors.

Ethics statement

The study was conducted in accordance with the Declaration of Helsinki (as revised in 2013). The study was approved by the ethics committee of the Children's Hospital, Zhejiang University School of Medicine (2021-IRB-097) and individual consent for this retrospective analysis was waived.

Author contributions

X-HM and JY designed this project and took charge of the development of machine learning and writing this paper. H-CZ and XJ delineated the area of interest in our medical images. J-WL and Y-SD had equal contributions in preparing figures and clinical information. TN and QS supervised the development of this project and guided the writing of this article. X-HM and JY takes mainly responsibility for the integrity of the content of the paper and each author have participated sufficiently in the submission to take public responsibility for the content. All authors contributed to the article and approved the submitted version.

Funding

This work was supported by Beijing Natural Science Foundation (Z210008) and Medical Health Science and Technology Project of Zhejiang Province (2022492239).

Conflict of interest

The authors declare that the research was conducted in the absence of any commercial or financial relationships that could be construed as a potential conflict of interest.

Publisher's note

All claims expressed in this article are solely those of the authors and do not necessarily represent those of their affiliated organizations, or those of the publisher, the editors and the reviewers. Any product that may be evaluated in this article, or claim that may be made by its manufacturer, is not guaranteed or endorsed by the publisher.

References

1. PDQ Pediatric Treatment Editorial Board. Wilms' Tumor and Other Childhood Kidney Tumors Treatment (PDQ®): Health Professional Version. (2022) Dec 23. In: PDQ Cancer Information Summaries [Internet]. Bethesda (MD): National Cancer Institute (US). (2002).
2. Cunningham ME, Klug TD, Nuchtern JG, Chintagumpala MM, Venkatramani R, Lubega J, et al. Global disparities in wilms tumor. *J Surg Res* (2020) 247:34–51. doi: 10.1016/j.jss.2019.10.044
3. Leslie SW, Sajjad H, Murphy PB, Tumor. W. *StatPearls*. Treasure Island (FL: StatPearls Publishing LLC (2022).
4. Lopes RI, Lorenzo A. Recent advances in the management of wilms' tumor. *F1000Res* (2017) 6:670. doi: 10.12688/f1000research.10760.1
5. Cozzi DA, Ceccanti S, Cozzi F. Renal function recovery after nephrectomy or nephron-sparing surgery in children with unilateral renal tumor. *Eur J Pediatr Surg* (2017) 27(1):74–80. doi: 10.1055/s-0036-1587336
6. Cost NG, Sawicz-Birkowska K, Kajbafzadeh AM, Tourchi A, Parigi GB, Guillén G, et al. A comparison of renal function outcomes after nephron-sparing surgery and radical nephrectomy for nonsyndromic unilateral wilms tumor. *Urology* (2014) 83(6):1388–93. doi: 10.1016/j.urol.2014.01.051
7. Haecker FM, von Schweinitz D, Harms D, Buerger D, Graf N. Partial nephrectomy for unilateral wilms tumor: results of study SIOP 93-01/GPOH. *J Urol* (2003) 170(3):939–42. doi: 10.1097/01.ju.0000073848.33092.c7
8. Wilde JC, Aronson DC, Sznajder B, Van Tinteren H, Powis M, Okoye B, et al. Nephron sparing surgery (NSS) for unilateral wilms tumor (UWT): the SIOP 2001 experience. *Pediatr Blood Cancer* (2014) 61(12):2175–9. doi: 10.1002/pbc.25185
9. Godzinski J, Graf N, Audry G. Current concepts in surgery for wilms tumor—the risk and function-adapted strategy. *Eur J Pediatr Surg* (2014) 24(6):457–60. doi: 10.1055/s-0034-1396425
10. Lambin P, Rios-Velazquez E, Leijenaar R, Carvalho S, van Stiphout RG, Granton P, et al. Radiomics: extracting more information from medical images using advanced feature analysis. *Eur J Cancer* (2012) 48(4):441–6. doi: 10.1016/j.ejca.2011.11.036
11. Liang C, Cheng Z, Huang Y, He L, Chen X, Ma Z, et al. An MRI-based radiomics classifier for preoperative prediction of ki-67 status in breast cancer. *Acad Radiol* (2018) 25(9):1111–7. doi: 10.1016/j.acra.2018.01.006
12. Aerts HJ, Velazquez ER, Leijenaar RT, Parmar C, Grossmann P, Carvalho S, et al. Decoding tumour phenotype by noninvasive imaging using a quantitative radiomics approach. *Nat Commun* (2014) 5:4006. doi: 10.1038/ncomms5006
13. Yang J, Wu Q, Xu L, Wang Z, Su K, Liu R, et al. Integrating tumor and nodal radiomics to predict lymph node metastasis in gastric cancer. *Radiother Oncol* (2020) 150:89–96. doi: 10.1016/j.radonc.2020.06.004
14. Liu Z, Wang S, Dong D, Wei J, Fang C, Zhou X, et al. The applications of radiomics in precision diagnosis and treatment of oncology: opportunities and challenges. *Theranostics* (2019) 9(5):1303–22. doi: 10.7150/thno.30309
15. Zhao L, Gong J, Xi Y, Xu M, Li C, Kang X, et al. MRI-Based radiomics nomogram may predict the response to induction chemotherapy and survival in locally advanced nasopharyngeal carcinoma. *Eur Radiol* (2020) 30(1):537–46. doi: 10.1007/s00330-019-06211-x
16. Zhang M, Zeng X, Huang C, Liu J, Liu X, Xie X, et al. An AI-based radiomics nomogram for disease prognosis in patients with COVID-19 pneumonia using initial CT images and clinical indicators. *Int J Med Inform* (2021) 154:104545. doi: 10.1016/j.ijmedinf.2021.104545
17. van Griethuysen JJM, Fedorov A, Parmar C, Hosny A, Aucoin N, Narayan V, et al. Computational radiomics system to decode the radiographic phenotype. *Cancer Res* (2017) 77(21):e104–7. doi: 10.1158/0008-5472.Can-17-0339
18. Wang X, Zhao X, Li Q, Xia W, Peng Z, Zhang R, et al. Can peritumoral radiomics increase the efficiency of the prediction for lymph node metastasis in clinical stage T1 lung adenocarcinoma on CT? *Eur Radiol* (2019) 29(11):6049–58. doi: 10.1007/s00330-019-06084-0
19. Meng X, Xia W, Xie P, Zhang R, Li W, Wang M, et al. Preoperative radiomic signature based on multiparametric magnetic resonance imaging for noninvasive evaluation of biological characteristics in rectal cancer. *Eur Radiol* (2019) 29(6):3200–9. doi: 10.1007/s00330-018-5763-x
20. Pudil P, Novovičová J, Kittler J. Floating search methods in feature selection. *Pattern Recognition Lett* (1994) 15(11):1119–25. doi: 10.1016/0167-8655(94)90127-9
21. Yip SS, Aerts HJ. Applications and limitations of radiomics. *Phys Med Biol* (2016) 61(13):R150–166. doi: 10.1088/0031-9155/61/13/r150
22. Chalkidou A, O'Doherty MJ, Marsden PK. False discovery rates in PET and CT studies with texture features: a systematic review. *PLoS One* (2015) 10(5):e0124165. doi: 10.1371/journal.pone.0124165
23. Yang J, Xu L, Yang P, Wan Y, Luo C, Yen EA, et al. Generalized methodology for radiomic feature selection and modeling in predicting clinical outcomes. *Phys Med Biol* (2021) 66(21). doi: 10.1088/1361-6560/ac2ea5
24. Wang J, Li M, Tang D, Gu W, Mao J, Shu Q. Current treatment for wilms tumor: COG and SIOP standards. *World J Pediatr Surg* (2019) 2(3):e000038. doi: 10.1136/wjps-2019-000038
25. Zhao Y, Liu G, Sun Q, Zhai G, Wu G, Li ZC. Validation of CT radiomics for prediction of distant metastasis after surgical resection in patients with clear cell renal cell carcinoma: exploring the underlying signaling pathways. *Eur Radiol* (2021) 31(7):5032–40. doi: 10.1007/s00330-020-07590-2
26. Parmar C, Grossmann P, Bussink J, Lambin P, Aerts H. Machine learning methods for quantitative radiomic biomarkers. *Sci Rep* (2015) 5:13087. doi: 10.1038/srep13087
27. Dong J, Li L, Liang S, Zhao S, Zhang B, Meng Y, et al. Differentiation between ependymoma and medulloblastoma in children with radiomics approach. *Acad Radiol* (2021) 28(3):318–27. doi: 10.1016/j.acra.2020.02.012
28. Hekmatian E, Jafari-Pozve N, Khorrami L. The effect of voxel size on the measurement of mandibular thickness in cone-beam computed tomography. *Dent Res J (Isfahan)* (2014) 11(5):544–8.